

Switched Vector Field-based Guidance for General Reference Path Following in Planar Environment

Subham Basak¹ and Satadal Ghosh²

Abstract—Reference path following is a key component in the functioning of almost all engineered autonomous agents. Among several path following guidance methods in existing literature, vector-field-based guidance approach has got wide attention because of its simplicity and guarantee of stability under a broad class of scenarios. However, the usage of same cross-track-error-dependent structure of desired vector field in most of the existing literature irrespective of instantaneous cross-track error and course angle of unmanned vehicle makes it quite restrictive in attaining faster convergence and also leads to infeasibly high turn rate command for many scenarios. To this end, this paper presents a novel switched vector field-based guidance for following a general reference path, in which the structure of the desired vector field depends on instantaneous cross-track-error and vehicle's course angle. While the developed method ensures faster convergence, it also ensures that the guidance command always stays within a realistic threshold satisfying its curvature constraint, thus making it more real-life implementable for autonomous vehicles with kino-dynamic constraints. Theoretical analysis for convergence of the developed guidance scheme is presented. Possibilities of undesirable chattering at phase transitions are also eliminated. Numerical simulation studies are presented to validate the satisfactory performance of the developed algorithm.

I. INTRODUCTION

With the steady advances in technologies related to autonomy, unmanned vehicles (UxVs) have seen large-scale adoption in different civilian and military applications. Capability of autonomously following pre-defined reference paths is a key component in most of these scenarios.

In existing literature, path following problem has been addressed in three broad ways - control theoretic, guidance theoretic and vector field-based methods [1]. Among control-theoretic methods, linear controllers like proportional-integral-derivative (PID) [2] and optimal control-based methods [3], [4] on linearized geometries have been presented for developing path following control schemes. However, these methods majorly rely on small deviation from nominal assumption that is valid for sufficiently small heading error or cross-track error geometries. Lyapunov-based nonlinear controllers have also been developed in [5], [6] for regulation of path following error. While these nonlinear control techniques possess guaranteed stability and reliable tracking, the guidance commands are complicated, model-dependent and also depend on the magnitude of error [7], which was resolved in differential geometry-based path following guidance formulations in [7], [8]. However, their convergence proofs were restricted to constant-curvature

planar paths. On the other hand, guidance-theoretic path following methods are model-independent, simple and easy to implement. Some of these schemes involve Pure pursuit (PP) [9], [10], line-of-sight (LOS) guidance [11], trajectory shaping guidance [12], combination of PP and LOSG [13]. Apart from these, A Proportional Navigation (PN)-resembling guidance was devised in [14] for following a virtual target at a fixed-look-ahead distance on a reference path (straight line or circular or perturbed path), while another PN-based guidance was formulated in [15] for following a virtual target at a fixed look-ahead direction. Apart from these, Dubins curve-based guidance scheme for following an optimal feasible path in three-dimensional space was presented in [16]. Among all these nonlinear formulations, the look-ahead-based path following guidance [14] has got popularity because of its simplicity and ease in application, asymptotic stability and robustness. However, its drawback of constant look-ahead distance makes it restrictive for realistic path following applications. To this end, a radius of reference path curvature-dependent variable look-ahead distance guidance was presented in [17]. The major limitation of the look-ahead-based guidance schemes is that the initial position of the UxV needs to be inside the range of specified look-ahead distance from the reference path, thus necessitating an additional mid-course guidance law if the initial position is outside of the look-ahead distance.

In this context, Vector field-based methods [18], are gainfully leveraged due to their low cross-track error and low control effort compared to other existing path following algorithms [1]. Following this approach, the desired course angle of the UxV is constructed using a vector field, whose integral curves asymptotically direct the UxV to the pre-determined reference path. Stability analysis of the vector field-based path-following method for reference straight and circular paths was presented in [18], while this method was extended in [19] to following a general reference path with small straight line approximation. In [20], a notion of circular attractor Lyapunov function was defined to generate the vector field for a reference path following. Distance-based application of irrotational and rotational parts of a vector field was utilized in [21] for path following in 3-D. A general method for creating the vector field needed for navigation in n-dimensional space was presented in [22], singularity problem of which was subsequently addressed in [23].

However, in most of the vector field-based methods in existing literature, the field is defined as a function of only cross-track error, thus making the vector field form same irrespective of the magnitude of cross-track error. This

The authors are with the Department of Aerospace Engineering, Indian Institute of Technology Madras, Chennai-600036, India, ae20d412@smail.iitm.ac.in, satadal@iitm.ac.in

significantly limits the possibility of enhanced convergence to the reference path. Moreover, in these formulations, as the cross-track error approaches to infinity, the commanded desired heading angle approaches to a constant, which often leads to kino-dynamically infeasible high turn rate command if the course angle error is very high. Additionally, curvature constraints play a pivotal role in achieving precise trajectory tracking and optimizing vehicle performance while taking real-world limitations into account [24]. To address all these considerations, in this paper, a general reference path following guidance scheme for planar applications is presented based on a novel formulation of switched vector field, in which its dependence on cross-track error facilitates in augmented convergence of the developed guidance scheme, while its dependence on UAV course ensures that the turn rate command remains within a kino-dynamically feasible threshold. Stability analysis for finite time convergence by the developed guidance strategy is given. Thus, attaining a faster path following while maintaining the guidance command within feasible threshold value forms the salient feature of the developed guidance scheme.

The rest of this paper is organized as follows: Section II defines the problem. Section III introduces different vector fields and develops as well as analyzes a novel guidance strategy for a following general reference path. Section III-D delves into the curvature limitations associated with general reference path following. The proposed guidance law is then validated using numerical simulations in Section IV. Finally, Section V concludes the overall guidance algorithm.

II. PROBLEM DEFINITION

A. Navigation Dynamics

Consider the problem of following a reference path as shown in Fig. 1. The navigational dynamics of a constant speed UAV flying at a constant altitude can be stated as,

$$\dot{x} = V_g \cos(\chi); \quad \dot{y} = V_g \sin(\chi); \quad \dot{\chi} = \alpha(\chi^c - \chi) \quad (1)$$

Here, $\mathbf{p} = [x, y]^T$ denotes the UAV's position w.r.t. inertial reference frame ($O - X_I, Y_I$). Its ground speed and course angle are given as $V_g = \sqrt{(V_{ax} + W_x)^2 + (V_{ay} + W_y)^2}$ and $\chi = \tan^{-1}((V_{ay} + W_y)/(V_{ax} + W_x))$, respectively, where V_a , W denote the UAV airspeed and wind speed, respectively. Subscripts x and y denote along X_I and Y_I directions. Incorporation of ground speed (V_g) and course of the UAV (χ) in (1) ensures that the wind-effect is implicitly factored in [18]. The UAV's guidance command is given by the turn rate ($\dot{\chi}$), where α is a positive constant, and χ^c represents the input course command generated by the guidance law for the UAV to follow a desired general path with time-efficiency, turn rate feasibility and path curvature constraint.

B. Definitions Related to Reference Path

In this paper, the closest point on the reference path from the UAV's current position \mathbf{p} is considered as the reference point (\mathbf{p}_{ref}). And, the distance from \mathbf{p} to \mathbf{p}_{ref} , represents the cross-track error $d = \rho||d||$, where, $\rho = \pm 1$ represents the side of the reference path the UAV is lying on. For example,

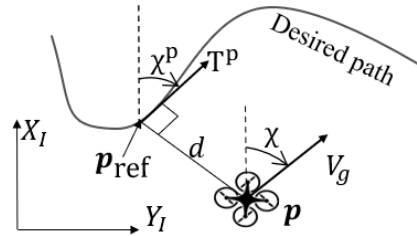


Fig. 1: General reference path following geometry

in Fig. 1, $\rho = +1$ as the UAV is on right side of the reference path. The tangent vector to the path at \mathbf{p}_{ref} is denoted as \mathbf{T}^p , which is perpendicular to \mathbf{d} . Here,

$$\dot{d} = V_g \sin(\chi - \chi^p) \quad (2)$$

and, χ^p is the angle between \mathbf{T}^p and X_I -axis.

III. GUIDANCE FOR GENERAL REFERENCE PATH FOLLOWING

In this section, a guidance strategy is formulated for an UAV to follow a general reference path based on a novel switched vector field-based method leading to enhanced performance in terms of path following time, while also satisfying feasible turn rate and path curvature constraints.

A. Vector Field Description

1) Dependence of Vector Field on Cross-track Error:

The vector field should be such that when the UAV is far away from the desired path (large $|d|$), the desired course is directed towards the path with a constant course angle $\chi^p - \chi^\infty$, and as $|d|$ approaches zero, the desired course aligns with the desired path. To achieve this, for general reference path following, the desired vector field is considered as follows.

$$\chi^d(d) = \chi^p - \chi^\infty (2/\pi) \tan^{-1}(k_i d^i) \quad (3)$$

where, $i = 2n+1$ and n is an integer, k_i is a positive constant that affects the rate of transition from χ^∞ to χ^p while guiding the UAV to reach the desired path asymptotically. Note that the vector field considered in [18], [19] is a special Case of Eq. (3) with $i = 1$. When the UAV is able to follow the vector field accurately, that is $\chi = \chi^d(d)$, from (2),

$$\frac{d(d)}{dt} = V_g \sin(\chi^d(d) - \chi^p) = -V_g \sin(\chi^\infty \frac{2}{\pi} \tan^{-1}(k_i d^i)).$$

Note that for higher value of i , when $|d|$ is large, $|\dot{d}|$ is also higher thus enabling the UAV to come closer to the desired path smoothly at a faster rate. But, when $|d|$ is very small, say d is within the interval $(-d_s, d_s)$ (shown as (p_1, p_2) in Fig. 2a), $|\dot{d}|$ is highest for $i = 1$. Then, cross-track error-dependent switching of vector field could be considered at $d = \rho d_s$ to ensure faster convergence. Now, for $\chi = \chi^d$,

$$\frac{d\chi^d(d)}{dt} = \dot{\chi}^p - \chi^\infty \frac{2}{\pi} \frac{ik_i d^{i-1}}{1 + (k_i d^i)^2} V_g \sin(\chi^\infty \frac{2}{\pi} \tan^{-1}(k_i d^i)).$$

Here, as i increases, $|\dot{\chi}^d(d) - \dot{\chi}^p|$ also increases for large $|d|$, which in turn demands high turn rate of the UAV. This is

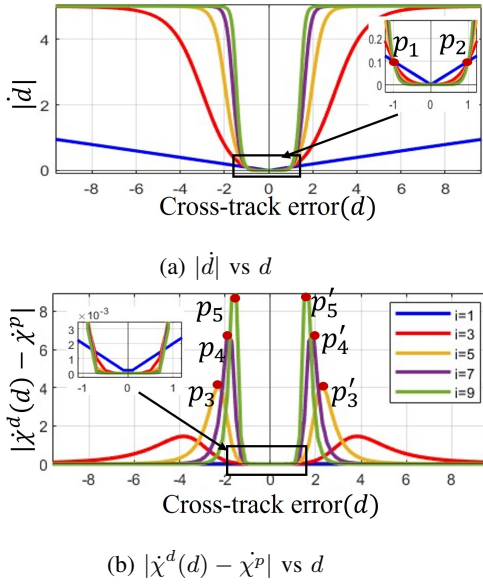


Fig. 2: Variation of $|\dot{d}|$ and $|\dot{\chi}^d(d) - \dot{\chi}^p|$, for $i = 1, 3, 5, 7, 9$.

illustrated in Fig. 2b. For $i > 3$, turn rate command becomes excessively high, which is often infeasible (see p_3, p_4, p_5 and p'_3, p'_4, p'_5 points in Fig. 2b).

Thus, to mitigate these issues while also deriving the advantage of both the formulations of $\chi^d(d)$ with $i = 1$ and $i = 3$, a switching mechanism is considered in the vector field formulation based on whether $|d|$ is greater or less than d_s , which ensures the UAV to converge with the desired path smoothly at a faster convergence rate without requiring infeasibly high turn rate. Thus, $i = 3$ is considered for $|d| \geq d_s$, and $i = 1$, else. In order to attain a continuous profile of $\chi^d(d)$, the convergence rate controlling parameters k_1 and k_3 are so chosen that at $d = \rho d_s$, the $\chi^d(d)$ is same for both $i = 1$ and $i = 3$. This implies that $d_s = \sqrt{k_1/k_3}$. Thus, the switched vector field based on cross-track error is expressed in terms of the desired UAV course as,

$$\chi^d(d) = \begin{cases} \chi^p - \chi^\infty (2/\pi) \tan^{-1}(k_3 d^3) & \text{if } |d| > d_s \\ \chi^p - \chi^\infty (2/\pi) \tan^{-1}(k_1 d) & \text{if } |d| \leq d_s \end{cases} \quad (4)$$

Note that following (4), $\chi^d(d)$ approaches to $\chi^p - \chi^\infty$ and χ^p as d approaches ∞ and zero, respectively.

2) *Dependence on Instantaneous UAV Course Angle (χ):* When $|\chi - \chi^d(d)|$ is very high, as illustrated in Fig. 3, then the generated guidance command also becomes very high. This problem becomes more severe when $|d| > d_s$ as more aggressive turn rate command is generated by using the formulation of $\chi^d(d)$ with $i = 3$ than that with $i = 1$. In order to get rid of this problem, χ also needs to be incorporated in the formulation of $\chi^d(d)$. Hence, the switched vector field, based on current course angle becomes,

$$\chi^d(d, \chi) = \begin{cases} \chi^d(d) + \rho \frac{\pi}{2}, & \text{if } |d| > d_s, |\chi - \chi^d(d)| > \frac{\pi}{2} \\ \chi^d(d) & \text{else} \end{cases} \quad (5)$$

where, $\chi^d(d)$ is as given in (4). Note from Fig. 3 that the selection of $\chi^d(d, \chi)$ in (5) above leads to less turn rate

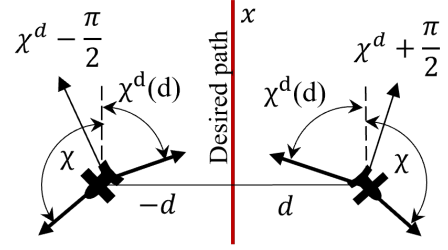


Fig. 3: Course angle based vector field for $\chi^p = 0$

command than $\chi^d(d)$ in (4) by decreasing $|\chi - \chi^d(d, \chi)|$ for $|\chi - \chi^d(d)| > \pi/2$. This, in effect, helps in ensuring that the commanded turn rate is within the upper threshold that arises from kino-dynamic constraints of a real unmanned vehicle.

B. Overall Guidance Strategy

Based on the discussion in Section III-A, the overall structure of the novel switched vector field is presented in terms of desired course angle expressed as a function of both cross-track error and course angle of the UAV as,

$$\chi^d(d, \chi) = \begin{cases} \chi^d(d) + \rho \frac{\pi}{2} = \chi^p - \chi^\infty \frac{2}{\pi} \tan^{-1}(k_3 d^3) + \rho \pi/2, & \text{if } |d| > d_s, |\chi - \chi^d(d)| > \pi/2; \\ \chi^d(d) = \chi^p - \chi^\infty \frac{2}{\pi} \tan^{-1}(k_3 d^3), & \text{if } |d| > d_s, |\chi - \chi^d(d)| \leq \pi/2; \\ \chi^d(d) = \chi^p - \chi^\infty \frac{2}{\pi} \tan^{-1}(k_1 d), & \text{if } |d| \leq d_s. \end{cases} \quad (6)$$

This desired vector field can be followed using the guidance command in (1), where the commanded UAV course χ^c is:

$$\chi^c = \begin{cases} \chi + \frac{\dot{\chi}^p}{\alpha} - \frac{1}{\alpha} \chi^\infty \frac{2}{\pi} \frac{3k_3 d^2}{1 + (k_3 d^3)^2} V_g \sin(\chi - \chi^p) - \rho \frac{\eta}{\alpha} (|\tilde{\chi}|)^{n/m}, & \text{if } |d| > d_s, |\chi - \chi^d(d)| > \frac{\pi}{2}; \\ \chi + \frac{\dot{\chi}^p}{\alpha} - \frac{1}{\alpha} \chi^\infty \frac{2}{\pi} \frac{3k_3 d^2}{1 + (k_3 d^3)^2} V_g \sin(\chi - \chi^p) - \frac{\beta}{\alpha} \text{sign}(\tilde{\chi}), & \text{if } |d| > d_s, |\chi - \chi^d(d)| \leq \frac{\pi}{2}; \\ \chi + \frac{\dot{\chi}^p}{\alpha} - \frac{1}{\alpha} \chi^\infty \frac{2}{\pi} \frac{k_1}{1 + (k_1 d)^2} V_g \sin(\chi - \chi^p) - \frac{\beta}{\alpha} \text{sign}(\tilde{\chi}), & \text{if } |d| \leq d_s. \end{cases} \quad (9)$$

where, $\tilde{\chi} \triangleq \chi - \chi^d(d, \chi)$. And, m, n are odd and co-prime integers such that $0 < n < m$. And, $\beta = \sigma / (1 + |\tilde{\chi}|)$, where $\sigma > 0$. Here, β and $\eta (> 0)$ control the shape of the trajectories onto the sliding surface $\tilde{\chi} = 0$.

C. Convergence Analysis

Consider $\chi^\infty = \pi/2$ and the scenario $d > 0$. The convergence analysis for the path following engagement geometries mentioned in (9)-(11) is given below. The analysis for $d < 0$ scenario would follow in similar way.

1) *Case - 1* ($|d| > d_s$ and $|\chi - \chi^d(d)| > (\pi/2)$): In this Case, the desired vector field in terms of $\chi^d(d, \chi)$ is as given in (6), and the commanded course angle χ^c as mentioned in (9). For this geometry, the course error $\tilde{\chi} = \chi - \chi^d(d, \chi)$ is guaranteed to decrease to zero in finite time as proved below.

Proposition 1: When $|d| > d_s$ and $|\chi - \chi^d(d)| > (\pi/2)$, where $\chi^d(d, \chi) = \chi^d(d) + \pi/2$ as given in (6), applying χ^c command as given in (9) brings $\tilde{\chi}$ to zero in finite time.

Proof: Following $\dot{\chi}$ from (1) and considering a Lyapunov candidate function $W_1 = \tilde{\chi}^2/2$.

$$\dot{W}_1 = \tilde{\chi}\dot{\tilde{\chi}} = \tilde{\chi}(\alpha(\chi^c - \chi) - \dot{\chi}^d(d, \chi)) \quad (12)$$

Considering $\chi^d(d, \chi)$ as in (6) for Case - 1, we obtain,

$$\dot{\chi}^d(d, \chi) = \dot{\chi}^p - \chi^\infty \frac{2}{\pi} \frac{3k_3 d^2}{1 + (k_3 d^3)^2} V_g \sin(\chi - \chi^p) \quad (13)$$

Then, applying χ^c as in (9), from (12), (13), it follows that, in Case-1, where $\tilde{\chi} = \chi - \chi^d(d, \chi) > 0$,

$$\dot{W}_1 = -\eta \tilde{\chi}(\tilde{\chi})^{n/m} < 0; \quad \dot{\tilde{\chi}} = -\eta(\tilde{\chi})^{n/m} < 0 \quad (14)$$

Here, for odd and co-prime n, m with $0 < n < m$, $\tilde{\chi}^{n/m}$ has one real solution with same sign as $\tilde{\chi}$, which implies from (14) that $\tilde{\chi}$ monotonically decreases and converges to zero in finite time $t_s = (m/(\eta(m-n)))|\tilde{\chi}(0)|^{(m-n)/m}$ [25]. This completes the proof of Proposition 1. ■

Remark 1: As $\chi^d(d) - \chi^p \in (-\pi/2, 0)$ for $\chi^\infty = \pi/2$ (refer to (4)), and $\chi - \chi^d(d) > \pi/2$ in Case - 1 geometry, we have $\chi - \chi^p \in (\pi/2, \pi)$. Then, from (2), $\dot{d} = V_g \sin(\chi - \chi^p) > 0$ implying that, $|d|$ increases with time for this geometry. Even at $t = t_s$, although $\chi(t_s) - \chi_{t_s}^d(d) = \pi/2$, we obtain $\chi(t_s) - \chi^p(t_s) \in (0, \pi/2)$ leading to positive $\dot{d}(t_s)$.

2) *Case - 2* ($|d| \geq d_s$ and $|\chi - \chi^d(d)| \leq \pi/2$): Proposition 1 guarantees finite time completion of Case-1 geometry, leading to Case-2 geometry, for which $\chi^d(d, \chi)$ and χ^c are switched to (7) and (10), respectively. Recall from Remark 1 that $\dot{d}(t_s) > 0$, therefore, d increases at the time of phase transition from Case - 1 to Case - 2. However, as $\tilde{\chi} = \chi - \chi^d(d, \chi)$ is shown to monotonically decrease in this case, χ crosses χ^p at some finite time, and $|d|$ also decreases then onward.

Proposition 2: When $|d| \geq d_s$ and $|\chi - \chi^d(d)| \leq \pi/2$, where $\chi^d(d, \chi) = \chi^d(d)$ as in (7), applying χ^c command given in (10) leads $\tilde{\chi}$ converge to zero in finite time.

Proof: Following $\dot{\chi}$ from (1) and considering a Lyapunov candidate function $W_2 = \tilde{\chi}^2/2$,

$$\dot{W}_2 = \tilde{\chi}\dot{\tilde{\chi}} = \tilde{\chi}(\alpha(\chi^c - \chi) - \dot{\chi}^d(d)) \quad (15)$$

From (7), for Case - 2 geometry we obtain,

$$\dot{\chi}^d(d, \chi) = \dot{\chi}^p - \chi^\infty \frac{2}{\pi} \frac{3k_3 d^2}{1 + (k_3 d^3)^2} V_g \sin(\chi - \chi^p) \quad (16)$$

Then, applying the commanded course χ^c as presented in (10), it follows from (15) and (16) that for Case-2,

$$\dot{W}_2 = -\beta \tilde{\chi} \text{sign}(\tilde{\chi}) < 0 \implies \dot{W}_2 \leq -\beta |\sqrt{W_2}|. \quad (17)$$

Therefore, it is evident that $|\tilde{\chi}|$ monotonically decreases and finally converges to zero in finite time [26]. ■

However, in practice, the $\text{sign}(\cdot)$ function in (10) leads to chattering in the control output [26]. To mitigate this, the $\text{sign}(\cdot)$ function can be replaced with $\text{sat}(\cdot)$ function. Therefore, the updated command is given as

$$\chi^c = \chi + \frac{\dot{\chi}^p}{\alpha} - \frac{1}{\alpha} \chi^\infty \frac{2}{\pi} \frac{3k_3 d^2}{1 + (k_3 d^3)^2} V_g \sin(\chi - \chi^p) - \frac{\beta}{\alpha} \text{sat}\left(\frac{\tilde{\chi}}{\epsilon}\right), \quad (18)$$

where, $\text{sat}(x)$ is defined as $\text{sat}(x) = x$ if $|x| \leq 1$, and $\text{sat}(x) = \text{sign}(x)$, else. And, $\epsilon > 0$ sets the boundary region width around the sliding surface to reduce chattering in $\dot{\chi}$.

Remark 2: Even if Case-2 is initiated with $\chi - \chi^p \in (0, \pi/2)$, as $\tilde{\chi}$ monotonically decreases to zero in finite time, as shown in Proposition 2, and as $\chi^d(d) - \chi^p \in (-\pi/2, 0)$ for $\chi^\infty = \pi/2$ (refer to (4)), $\chi - \chi^p$ also lies in the interval $(-\pi/2, 0)$ as $\chi \rightarrow \chi^d(d)$. Besides, as $\dot{\chi}$ is continuous within the time interval the geometry lies in Case - 2, by intermediate value theorem, $\chi - \chi^p$ is guaranteed to cross zero in a finite time. And, that time onward, $\dot{d} = V_g \sin(\chi - \chi^p) < 0$ implying monotonically decreasing $|d|$.

Remark 3: From (14), $\dot{\tilde{\chi}} = 0$ at $t = t_s$ as $\tilde{\chi}(t_s) = 0$ for $\tilde{\chi} = \chi - \chi^d(d, \chi)$ in Case - 1. Hence, if the switching of vector field at the transition from Case - 1 to Case - 2 takes place at $t = t_s$, there is a possibility of undesirable chattering at the transition. To avoid that, this switching may be done at $t = t_s - \epsilon_t$ for some small positive ϵ_t , when $|\chi - \chi^d| = (\pi/2) + \Delta$ for some small positive Δ . Note that since \dot{d} and $\dot{\tilde{\chi}}$ remain positive and negative, respectively, both at $t = t_s - \epsilon_t$ (follows Case - 1) and at the beginning of Case - 2 geometry after the transition, the switching at $t = t_s - \epsilon_t$ would maintain the same convergence pattern, while also ensuring no undesired chattering during the switching of vector field between Case -1 and Case - 2 geometries.

Proposition 3: When $|d| \geq d_s$ and $|\chi - \chi^d(d)| \leq \pi/2$, where $\chi^d(d, \chi) = \chi^d(d)$ as given in (7), applying χ^c as given in (10) as χ converges to $\chi^d(d)$, $|d|$ is guaranteed to monotonically decrease and reach d_s in finite time.

Proof: Define a Lyapunov candidate function $W_3 = d^2/2$. As χ converges to $\chi^d(d)$ (by Proposition 2), from (2),

$$\dot{W}_3 = d\dot{d} = -V_g d \sin(\chi^\infty (2/\pi) \tan^{-1}(k_3 d^3)) \quad (19)$$

Here, $\dot{W}_3 < 0$, and $\dot{d} \leq -V_g \sin(\chi^\infty \frac{2}{\pi} \tan^{-1}(k_3 d_s^3)) < 0$ for $|d| > d_s \neq 0$. This leads to finite time convergence of $|d|$ to d_s . Thus, the proposition holds. ■

3) *Case - 3* ($|d| < d_s$): Propositions 1, 2 and 3, guaranteed the path following guidance switches to this Case within finite time. Consequently, $\chi^d(d, \chi)$ and χ^c are switched to (8) and (11), respectively. Following the same steps as in Case - 2 in Section III-C.2, the following result can be shown.

Proposition 4: When $|d| < d_s$, where $\chi^d(d, \chi) = \chi^d(d)$ as given in (8), applying χ^c command as given in (11) leads $\tilde{\chi} = \chi - \chi^d(d, \chi)$ converge to zero in finite time, and as a consequence, d converges to zero asymptotically.

Remark 4: The transition from Case - 2 to Case -3 takes place at $d = d_s \neq 0$. Also, both at the end of Case - 2 and at the beginning of Case -3 geometries, both \dot{d} and $\dot{\chi}$ are negative. These eliminate the possibility of chattering and any degradation of convergence performance during the switching of vector field from Case -2 to Case - 3.

4) Final Result:

Theorem 1: Starting from any χ and d , the overall vector field given by (6),(7), (8), and the respective guidance command represented by (9),(10), and (11), guarantee that the UAV is able to follow the desired general reference path asymptotically and reaches its close vicinity in finite time.

Proof: From Propositions 1 - 4 and selecting $d_s = \sqrt{k_1/k_3}$ suitably by tuning control parameters k_1 and k_3 in (4), this result follows in a straight-forward way. ■

D. Curvature Constraints

Convergence analysis in Section III-C shows that convergence rate of χ to $\chi^d(d, \chi)$ depends on η , β and k_i (for $i = 1, 3$), as indicated by (14), (17) and (19), respectively. These parameters also affect the curvature of the UAV's path as may be noted from (1), (9)-(11). Accordingly, this section outlines conditions on these parameters to ensure kino-dynamic feasibility of the UAV's commanded path. For that, considering $\chi = \chi^d(d, \chi)$, the curvature variation is:

$$\kappa = d\chi/ds = d\chi^d(d, \chi)/ds = (d\chi^d(d, \chi)/dt)/(ds/dt). \quad (20)$$

For $|d| \leq d_s$, using $\chi^d(d, \chi)$ from (8) and $\chi^\infty = \pi/2$,

$$d\chi^d(d, \chi)/dt - \dot{\chi}^p = k_1^2 V_g d / (1 + (k_1 d)^2)^{3/2} \quad (21)$$

Note that $\dot{\chi}^p$ does not have dependence on $|d|$. Thus, the condition for maximum value of $\chi^d(d, \chi)$ is:

$$\nabla_d \chi^d(d) = k_1^2 V_g \cdot (1 - 2k_1^2 d^2) / (k_1^2 d^2 + 1)^{5/2} = 0 \quad (22)$$

From (22), for $|d| \leq d_s$, we obtain that $|\dot{\chi}^d(d, \chi) - \dot{\chi}^p|_{max} = (2/3\sqrt{3})k_1 V_g$ at $|d| = 1/(\sqrt{2}k_1)$. Similarly, recall that for $|d| > d_s$, $i = 3$, and $\chi^d(d, \chi)$ is given in (6) and (7). Then, at $|d| = \sqrt[5]{5/(\sqrt[3]{2}\sqrt[3]{k_3})}$, $|\dot{\chi}^d(d, \chi) - \dot{\chi}^p|_{max} = (2^{4/3} \cdot 5^{5/6} V_g \sqrt[3]{k_3})/9$. Now, for $\chi = \chi^d(d, \chi)$, from (20),

$$(|\dot{\chi}^d(d, \chi)|_{max})/V_g = \kappa_{max} \quad (23)$$

where, κ_{max} is the maximum allowable curvature in the UAV's path. Then, from (23),

$$\begin{aligned} |\dot{\chi}^d(d, \chi) - \dot{\chi}^p|_{max} &\leq |\dot{\chi}^p|_{max} + |\dot{\chi}^d(d, \chi)|_{max} \\ \implies |\dot{\chi}^d(d, \chi) - \dot{\chi}^p|_{max} - |\dot{\chi}^p|_{max} &\leq V_g \kappa_{max}. \end{aligned} \quad (24)$$

As, $|\dot{\chi}^d(d, \chi) - \dot{\chi}^p|_{max}$ dependent on the V_g , k_1 and k_3 as discussed above, (24) can be rewritten as,

$$\max \left\{ 2k_1/(3\sqrt{3}), (2^{4/3} \cdot 5^{5/6} \sqrt[3]{k_3})/9 \right\} - |\dot{\chi}^p|_{max}/V_g \leq \kappa_{max} \quad (25)$$

Thus, for given κ_{max} (UAV's turn rate constraint), $|\dot{\chi}^p|_{max}$ (maximum path curvature) and V_g (UAV speed), the overall switched vector field ((6)-(8)) can be designed by suitably selecting k_1 and k_3 that satisfies (25). This can be followed by the commanded course angles ((9)-(11)) with suitable

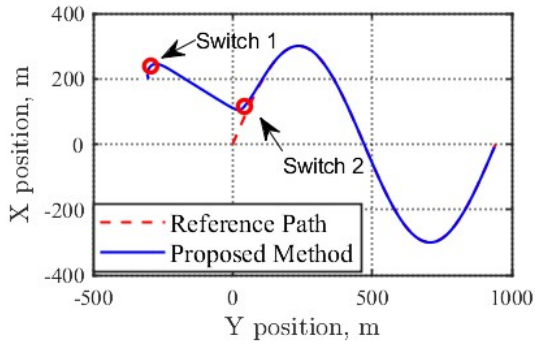
selection of η and β satisfying the κ_{max} constraint for effectively following a general reference path without any undesirable chattering at phase transitions, as explained in Theorem 1, Remarks 3 and 4.

IV. SIMULATION RESULTS

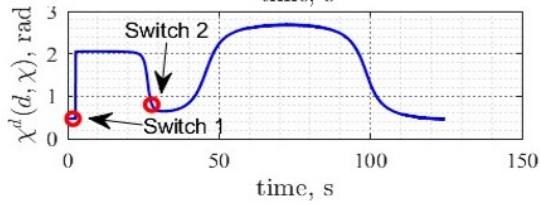
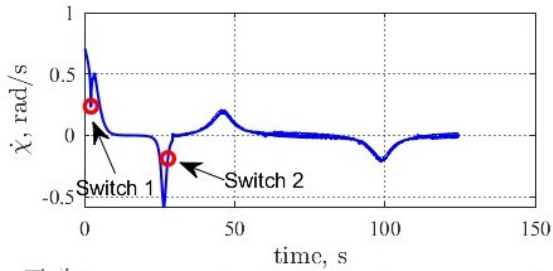
In this section, the path following guidance strategy presented in Section III-B is validated using numerical simulations performed in MATLAB (R2023a) environment. The parameters considered for the simulations are as follow. Constant UAV speed (V_a) of 15 m/s is considered for all scenarios. And, $\chi^\infty = \pi/2$, $\alpha = 1.65 \text{ s}^{-1}$, $\gamma = 0.8$, $\eta = \pi/4$ rad, $n = 3$, $m = 5$, $d_s = 10$ m, $k_1 = 0.01$, $k_3 = k_1/d_s^2 = 10^{-4}$. In practice, $\dot{\chi}^p$ can be approximated using tangents to the path as $\dot{\chi}^p \approx (\chi^p - \chi_{old}^p)/dt$, where χ_{old}^p is the tangent to the path in the previous time step.

Fig. 4 illustrates a numerical example of following a reference sinusoidal path ($y = r \sin(x)$, where $r = 300$ and $x \in [0, 2\pi]$) with no wind consideration, that is $V_g = V_a$, for better understanding of the convergence analysis given above. As can be seen in Fig. 4a, initially $d < d_s$ and also $|\chi - \chi^d(d)| > \pi/2$, i.e. the geometry is in Case - 1. As stated in Remark 1, $|d|$ increases initially as shown in Fig. 4d. However, from Fig. 4c, observe that $|\tilde{\chi}| = |\chi - (\chi^d(d) + \pi/2)|$ monotonically decreases as discussed in proposition 1. As it reaches near zero, the 1st switching happens as shown as Switch 1 in Fig. 4. At Switch 1, following Case - 2 geometry, the vector field has $\tilde{\chi} = \chi - \chi^d(d)$, which leads to a jump in $\tilde{\chi}$ profile (see Fig. 4c). Then, in line with Proposition 2 for Case - 2 geometry, $|\tilde{\chi}|$ monotonically decreases. After the transition from Case - 1 to Case - 2, initially $|d|$ is still greater than zero. As a result, $|d|$ increases initially in Case - 2 geometry. However, as χ crosses χ^p , then $|d|$ starts decreasing (see Fig. 4d) as per Remark 2. As $|d|$ crosses d_s in finite time (Proposition 3), Switch 2 happens, and the geometry falls in Case - 3, wherein following Proposition 4, $\tilde{\chi}$ and $|d|$ monotonically decrease. Besides, as mentioned in Remarks 3 and 4, no undesirable chattering is observed at the phase transitions. Now, from $\dot{\chi}$ profile in Fig. 4b, $|\dot{\chi}|_{max} = 0.7$ rad/sec, which is within kino-dynamically feasible range. This leads to RHS of (25) as $\kappa_{max} = |\dot{\chi}|_{max}/V_a = 0.046$ /m. And for the considered reference path, $|\dot{\chi}^p|_{max} = 0.1$ rad/sec. Therefore, LHS of (25) becomes 0.036, which satisfies (25).

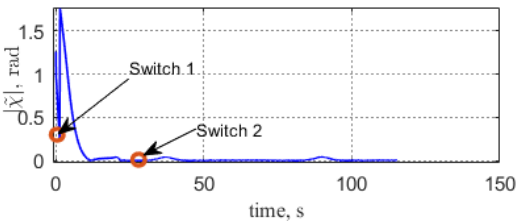
The developed guidance algorithm (a) is now compared with (b) vector field method [18], (c) PLOS method [13], and (d) NLGL (L_1) method [14], with parameters fine tuned for better performance as follows. For method (b) $k = 0.02$ and $\beta = \pi/2$, for (c) $K_1 = 15$ and $K_2 = 0.1$, and for (d) $L_1 = 110$ m. The initial conditions considered are $|d_0| = 200$ m (for (a), (b) and (c)), and $|d_0| = 80$ m (for (d)) and $\chi_0 = -\pi/4$ (for all methods). From Figs. 5a and 5b, note that Methods (b) and (c) closely follow the path, but initial turn rate command is very high for method (c), and the convergence time for method (b) is high. On the other hand, method (d) has always higher cross-track error. Unlike them, the proposed switched vector field method allows the



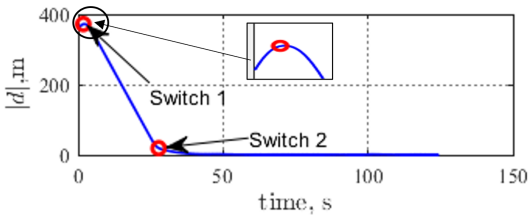
(a) UAV trajectory



(b) Desired vector field and $\dot{\chi}$

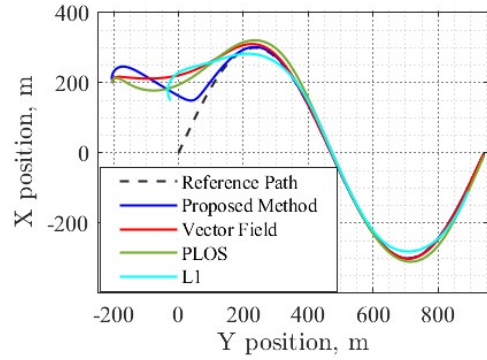


(c) $|\tilde{\chi}|$ profile

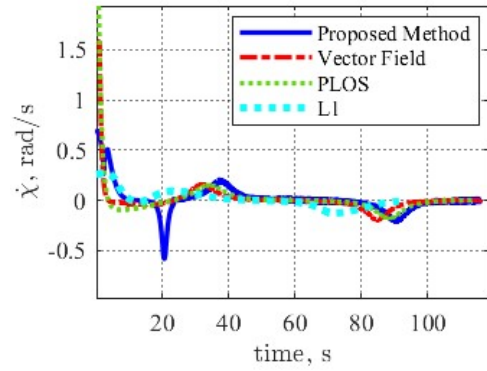


(d) Cross-track error magnitude

Fig. 4: Illustration of path following by the proposed switched vector field-based guidance.



(a) UAV trajectories



(b) Turn rate command

Fig. 5: Illustration of path following by the proposed method, vector field[18], PLOS[13] and NLGL (L_1) [14]

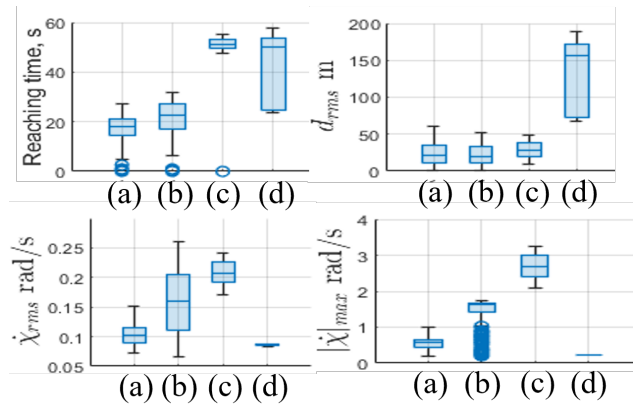


Fig. 6: Comparison of path following by the (a) proposed switched vector field, (b) vector field[18], (c) PLOS[13] and (d) NLGL(L_1) [14] under random initial condition by Box-plot representation of t_{conv} , d_{rms} , $\dot{\chi}_{rms}$, and $\max(|\dot{\chi}|)$.

UAV to closely follow the path with feasible turn rate and low convergence time.

Total 200 random trials are next performed with $d_0 \sim \mathcal{U}[100, 200]$ m, $\chi_0 \sim \mathcal{U}[-\pi, \pi]$ rad, wind speed, $|W| \sim \mathcal{U}[2, 3]$ m/s, wind direction $\sim \mathcal{U}[-2, -2.5]$ rad and control parameters same as previous simulations. The performance measures are: i) Reaching time (t_{conv}), ii) RMS cross track error (d_{rms}), iii) RMS turn rate, $\dot{\chi}_{rms}$ and iv) maximum turn rate, $\max(|\dot{\chi}|)$, as shown in Fig. 6. Here, t_{conv} is defined as the duration by which the UAV reaches a threshold distance relative to the reference path, while subsequently following a course angle sufficiently close to path's curvature. While the NLGL method [14] exhibits low $\dot{\chi}_{rms}$, its d_{rms} and t_{conv} are comparatively higher when compared to other methods. For PLOS method [13], d_{rms} is lower, but it has higher $\dot{\chi}_{rms}$, $|\dot{\chi}|_{max}$ and t_{conv} . Although the d_{rms} is almost similar for proposed switching vector field-based and the basic Vector field method [18], it is evident that the switched vector field-based approach significantly outperforms path-following methods in terms of all performance measures.

V. CONCLUSIONS

This paper has presented a cross-track-error and course angle-dependent novel switching strategy in defining the desired vector field for following a general reference path. Theoretical analysis on its convergence has been presented. The developed guidance scheme has been shown to ensure faster convergence, thus leading to a lesser reaching time, while it also ensures that the guidance command does not go beyond a threshold even when the course angle error is very high. Undesirable chattering at phase transitions is also avoided. Numerical simulation studies have been presented to justify the performance of the developed guidance algorithm. Comparison studies have shown the superiority of the presented method over other existing methods.

REFERENCES

- [1] P. Sujit, S. Saripalli, and J. B. Sousa, "Unmanned aerial vehicle path following: A survey and analysis of algorithms for fixed-wing unmanned aerial vehicles," *IEEE Control Syst. Magazine*, vol. 34, no. 1, pp. 42–59, 2014.
- [2] I. Rhee, S. Park, and C.-K. Ryoo, "A tight path following algorithm of an uas based on pid control," in *Proc. SICE Annual Conf. 2010*, 2010, pp. 1270–1273.
- [3] A. Ratnoo, P. Sujit, and M. Kothari, "Adaptive optimal path following for high wind flights," *IFAC Proc. Vol.*, vol. 44, no. 1, pp. 12985–12990, 2011.
- [4] S. He, C.-H. Lee, H.-S. Shin, and A. Tsourdos, "Minimum-effort waypoint-following guidance," *J. Guid. Control Dyn.*, vol. 42, no. 7, pp. 1551–1561, 2019.
- [5] C. Liu, O. McAree, and W.-H. Chen, "Path-following control for small fixed-wing unmanned aerial vehicles under wind disturbances," *Int. J. Robust Nonlinear Control*, vol. 23, no. 15, pp. 1682–1698, 2013.
- [6] G. Flores, I. Lugo-Cárdenas, and R. Lozano, "A nonlinear path-following strategy for a fixed-wing mav," in *Int. Conf. Unmanned Aircr. Syst.* IEEE, 2013, pp. 1014–1021.
- [7] N. Cho, Y. Kim, and S. Park, "Three-dimensional nonlinear differential geometric path-following guidance law," *J. Guid. Control Dyn.*, vol. 38, no. 12, pp. 2366–2385, 2015.
- [8] D. J. Gates, "Nonlinear path following method," *J. Guid. Control Dyn.*, vol. 33, no. 2, pp. 321–332, 2010.
- [9] E. D. Medagoda and P. W. Gibbens, "Synthetic-waypoint guidance algorithm for following a desired flight trajectory," *J. Guid. Control Dyn.*, vol. 33, no. 2, pp. 601–606, 2010.
- [10] J. Zhang, Q. Li, N. Cheng, and B. Liang, "Path-following control for fixed-wing unmanned aerial vehicles based on a virtual target," *Proc. Inst. Mech. Eng. G: J. Aerosp. Eng.*, vol. 228, no. 1, pp. 66–76, 2014.
- [11] R. Rysdyk, "Unmanned aerial vehicle path following for target observation in wind," *J. Guid. Control Dyn.*, vol. 29, no. 5, pp. 1092–1100, 2006.
- [12] A. Ratnoo, S. Y. Hayoun, A. Granot, and T. Shima, "Path following using trajectory shaping guidance," *J. Guid. Control Dyn.*, vol. 38, no. 1, pp. 106–116, 2015.
- [13] M. Kothari, I. Postlethwaite, and D.-W. Gu, "Uav path following in windy urban environments," *J. Intell. Robot. Syst.*, vol. 74, no. 3, pp. 1013–1028, 2014.
- [14] S. Park, J. Deyst, and J. P. How, "Performance and Lyapunov stability of a nonlinear path following guidance method," *J. Guid. Control Dyn.*, vol. 30, no. 6, pp. 1718–1728, 2007.
- [15] N. Dhananjay and R. Kristiansen, "Guidance strategy for gradient search by multiple uavs," in *AIAA Guid. Navig. Control Conf.*, 2012, p. 4766.
- [16] S. Hota and D. Ghose, "Rectilinear path following in 3d space," in *Trends in Intelligent Robotics: FIRA Robot World Congress*. Springer, 2010, pp. 210–217.
- [17] R. Saurav, L. D. Sohil, and S. Ghosh, "Variable H guidance strategy for path following of uavs," in *Int. Conf. Unmanned Aircr. Syst.*, 2020, pp. 1518–1524.
- [18] D. R. Nelson, D. B. Barber, T. W. McLain, and R. W. Beard, "Vector field path following for miniature air vehicles," *IEEE Trans. Robot.*, vol. 23, no. 3, pp. 519–529, 2007.
- [19] S. Griffiths, "Vector field approach for curved path following for miniature aerial vehicles," in *AIAA Guid. Navig. Control Conf.*, 2006, p. 6467.
- [20] D. A. Lawrence, E. W. Frew, and W. J. Pisano, "Lyapunov vector fields for autonomous unmanned aircraft flight control," *J. Guid. Control Dyn.*, vol. 31, no. 5, pp. 1220–1229, 2008.
- [21] Y. Liang and Y. Jia, "Combined vector field approach for 2d and 3d arbitrary twice differentiable curved path following with constrained uavs," *J. Intell. Robot. Syst.*, vol. 83, no. 1, pp. 133–160, 2016.
- [22] V. M. Goncalves, L. C. Pimenta, C. A. Maia, B. C. Dutra, and G. A. Pereira, "Vector fields for robot navigation along time-varying curves in n -dimensions," *IEEE Trans. Robot.*, vol. 26, no. 4, pp. 647–659, 2010.
- [23] W. Yao, H. G. de Marina, B. Lin, and M. Cao, "Singularity-free guiding vector field for robot navigation," *IEEE Trans. Robot.*, vol. 37, no. 4, pp. 1206–1221, 2021.
- [24] A. Shivam and A. Ratnoo, "Arcsine vector field for path following guidance," *J. Guid. Control Dyn.*, pp. 1–12, 2023.
- [25] X. Yu, Y. Wu, and M. Zhihong, "On global stabilization of nonlinear dynamical systems," *Variable structure systems, sliding mode and nonlinear control*, pp. 109–122, 1999.
- [26] Y. Shtessel, C. Edwards, L. Fridman, A. Levant *et al.*, *Sliding mode control and observation*. Springer, 2014, vol. 10.